JGR Space Physics

Key Points:
- A hybrid model is used to generate synthetic energy spectrograms of the thermal ions along close flybys through potential plumes at Europa
- Close to Europa, the visibility of a plume in these spectrograms is strongly affected by ion deflection around the moon's Alfvén wings
- Due to field line draping, a particle detector looking away from Europa may have the best chances of capturing signatures of a plume source

Correspondence to:
H. Arnold,
hannes.arnold@eas.gatech.edu

Applying Ion Energy Spectrograms to Search for Plumes at Europa

Hannes Arnold[1] , Sven Simon[1] , and Lucas Liuzzo[1,2]

[1]School of Earth and Atmospheric Sciences, Georgia Institute of Technology, Atlanta, GA, USA, [2]Space Sciences Laboratory, University of California, Berkeley, Berkeley, CA, USA

Abstract We constrain the diagnostic potential of ion energy spectrograms to identify signatures of water vapor plumes in the thermal plasma environment of Jupiter's moon Europa. For this purpose, we apply a hybrid model of Europa's Alfvénic plasma interaction to calculate the perturbations of the flow and the electromagnetic fields near the moon for various plume locations on its surface, combined with different sets of magnetospheric upstream conditions (corresponding to different distances between Europa and the center of Jupiter's plasma sheet). The model output is used to generate synthetic time series for the count rates of the observable thermal ion population as a function of energy along several hypothetical spacecraft trajectories as well as for the Galileo E26 flyby. We demonstrate that the observability of characteristic plume signatures depends strongly on the viewing direction of the detector. Most surprisingly, for certain plume locations, a particle detector facing away from Europa captures more clearly discernible signatures of a plume passage than a detector looking into the direction of the moon. This puzzling result is caused by the deflection of magnetospheric and plume ions near Europa's Alfvén wings as well as a "contamination" of the spectrograms by cold plasma from the moon's global exosphere. The signature of the plume crossed during E26 is most clearly visible for a detector orientation that simultaneously captures the cold plume ions and a portion of the incident magnetospheric ion population. The results of this study will facilitate the planning of synergistic measurements during upcoming missions to Europa.

1. Introduction

Based on induction signatures seen in Galileo magnetometer data, Kivelson et al. (2000) showed that Europa (radius $R_E = 1,560.8$ km) likely hosts a subsurface ocean with a depth on the order of 100 km. The thickness of Europa's icy crust proposed in the literature varies from a few kilometers up to 60 km (Hand & Chyba, 2007; Hussmann et al., 2002; Schenk, 2002). In December 2012, Hubble Space Telescope (HST) observations revealed an increase of ultraviolet emission in Europa's south polar region, which can be interpreted as a surplus of oxygen and hydrogen. Roth et al. (2014) demonstrated that this inhomogeneity in Europa's atmosphere is consistent with one or two water vapor plumes with a scale height of about 200 km. Both plumes are expected to have vertical outgassing speeds of 500–700 m/s at Europa's surface (Roth et al., 2014). Based on further image post-processing of HST data, Sparks et al. (2016, 2017) suggested the presence of two additional plume sources close to Europa's south pole and equator. However, this finding was recently put into question (Giono et al., 2020). An additional transient source of water vapor on Europa's surface was recently identified in data from the Keck Observatory (Paganini et al., 2019).

Orbiting at a distance of 9.38 R_J (radius of Jupiter $R_J = 71,492$ km), Europa is located within the Jovian plasma sheet (Kivelson et al., 2009) and magnetosphere (Smith et al., 1974). Because of Europa's large orbital period compared to Jupiter's rotational period, subsonic magnetospheric plasma continuously hits the moon's exosphere and ionosphere. The main mechanism behind the generation of Europa's thin molecular oxygen O_2 exosphere (Burger & Johnson, 2004; McGrath et al., 2009) is a combination of sputtering of its icy surface and radiolysis of the sputtered material by energetic particles (Cooper et al., 2001). The intensity of Europa's surface sputtering decreases from the moon's ramside to its wakeside (Breer et al., 2019; Cassidy et al., 2013; Pospieszalska & Johnson, 1989), which results in a denser atmosphere in the trailing hemisphere (that faces the plasma flow) compared to the leading (wakeside) hemisphere. Electron impact ionization (being an order of magnitude stronger than UV ionization, see Saur et al., 1999) partially ionizes

Europa's thin exosphere. The asymmetry in the global atmosphere therefore maps into the structure of Europa's ionosphere.

The interaction between the submagnetosonic plasma flow at Europa, the induced magnetic field, and the moon's ionosphere results in a "kink" in the magnetic field lines which propagates in both directions, northward and southward, along the field with the Alfvén velocity $v_A = |\vec{B}|/(\mu_0 \rho)^{1/2}$, where $|\vec{B}|$ is the magnitude of the magnetospheric field, ρ is the mass density of the plasma, and μ_0 the vacuum permeability. A system of non-linear standing Alfvén waves (called Alfvén wings) connects Europa to Jupiter's polar ionosphere (Neubauer, 1980, 1998). These wings carry currents that close within the moon's conducting ionosphere. A localized inhomogeneity in the atmosphere, due to, for example, the presence of a plume in Europa's southern hemisphere, will enhance the current density and flow deceleration within the main Alfvén wing (Arnold et al., 2019, 2020; Blöcker et al., 2016). This tube-like region of enhanced current density can extend to arbitrarily large distances from Europa (due to the translational invariance along the Alfvén wing characteristics, see Neubauer, 1980) and is referred to as an Alfvén winglet by Blöcker et al. (2016). Therefore, a plume at, for example, Europa's south pole, will break the symmetry of the Alfvén wings between the moon's northern and southern hemispheres. Jupiter's time-varying field at Europa induces a dipolar magnetic field in Europa's subsurface ocean (Khurana et al., 1998; Zimmer et al., 2000). Neubauer (1999) predicted, Volwerk et al. (2007) demonstrated (by analyzing Galileo Europa flyby data), and Arnold et al. (2020) confirmed (by using a hybrid plasma model) shrinking of the Alfvén wing cross sections due to Europa's induced magnetic field.

In addition to remote telescope observations, recent studies have attempted to use magnetic field and plasma data from the Galileo encounters to identify plumes at Europa. Out of 12 targeted Europa flybys, only two flybys—E12 (on 16 December 1997) and E26 (on 3 January 2000)—passed by Europa's surface at an altitude comparable to the plumes' scale height (closer than 400 km, see Roth et al., 2014). Blöcker et al. (2016) analyzed the magnetic field signatures observed during Galileo's E26 encounter by using a three-dimensional magnetohydrodynamic model. Their work led to novel findings regarding the physics of plume-plasma interactions (e.g., the concept of an Alfvén winglet) and also provided initial hints of a plume crossing during E26. Arnold et al. (2019) reanalyzed magnetic field data from the E26 flyby by using the hybrid model Adaptive Ion-Kinetic Electron-Fluid (AIKEF, see Müller et al., 2011). These authors were able to present strong evidence for a plume crossing by achieving good agreement with magnetic field data and by demonstrating that the observed fine structures in the magnetic field are not reproducible by simulations without a plume. Additional evidence for the crossing of a plume during E26 was recently found in energetic proton observations by Huybrighs et al. (2020). These authors demonstrated that charge exchange and ion deflection near the plume cause a local decrease in the count rates of protons in the 115–244 keV regime, as observed by Galileo. Further, Jia et al. (2018) analyzed magnetic field and plasma perturbations from the E12 flyby by using the BATS-R-US multifluid model. Similar to Arnold et al. (2019), they were able to present strong evidence for a plume crossing in magnetic field and, additionally, in plasma density data acquired around closest approach (C/A) of that flyby.

However, despite these findings, knowledge on the signatures that a plume would leave in in situ spacecraft data is still limited. In particular, magnetic field data are available only along the spacecraft's trajectory, the orientation of the magnetic background field is variable in time, and the locations of potential plumes across Europa's surface are largely unknown and probably transient (Paganini et al., 2019; Roth et al., 2014, 2016; Sparks et al., 2016). Therefore, Arnold et al. (2020) presented a systematic modeling framework for the identification of water vapor plumes in plasma and magnetic field data along hypothetical spacecraft flybys for different magnetospheric background field conditions, plume orientations, and exosphere models at Europa. In particular, Arnold et al. (2020) considered plumes at Europa's south pole as well as at the apices of the moon's leading and trailing hemispheres. They systematically investigated how the observable magnetic field perturbations change when, for example, the complexity of the model for Europa's global exosphere is increased or the induced dipole field from the subsurface ocean is taken into account. Overall, Arnold et al. (2020) found that localized regions of stagnant flow are most indicative of the presence of a plume and that the visibility of plumes in the magnetic field is highly dependent on the density profile of the global atmosphere. However, Arnold et al. (2020) mainly focused on the observable magnetic field perturbations and did not consider the imprint that potential plumes leave in, for example, the particle energy spectra typically acquired by plasma detectors aboard spacecraft. The goal of the present study is to close this gap in our understanding of plume-plasma interactions at Europa.

This study will build upon the work of Arnold et al. (2020). The hybrid model of Arnold et al. (2020) treats ions as individual (macro)particles, allowing us to analyze the kinetic energy distribution of particles in any given cell of the simulation domain (in contrast to fluid models of moon-plasma interactions, which need to make assumptions on the shape of the local velocity distribution). In this way, we can determine the ion energy distribution along hypothetical trajectories that intersect plumes at different surface locations, similar to the magnetic field signatures along synthetic trajectories discussed by Arnold et al. (2020). Unfortunately, thermal ion energy spectrograms from the Galileo E12 and E26 flybys are not available in the peer-reviewed literature, and the time resolution of the Galileo data sets is likely too coarse to further constrain any signatures of the plumes seen in magnetic field data. However, future missions (like, e.g., the Europa Clipper and the JUpiter Icy moons Explorer [JUICE]) may very well be able to acquire time series of the ion energy distribution that are sufficiently detailed to search for possible plume signatures. For Enceladus, it has already been shown that plumes are visible in thermal ion energy spectrograms obtained by the Cassini spacecraft (Tokar et al., 2009). Therefore, we will conduct a systematic search for characteristic signatures of cold plume plasma in our modeled energy spectrograms and provide a framework for identification of plume signatures in particle data for upcoming in situ flyby missions.

In their preceding studies, Arnold et al. (2019, 2020) have generated an extensive pool of hybrid plasma simulations for different upstream conditions, global exosphere models, and plume configurations at Europa. For this study, we shall select several hybrid model runs from that pool and use them to generate synthetic ion energy spectrograms. These spectrograms will then be applied to evaluate the challenges associated with the identification of plume signatures using in situ particle data.

This paper is organized as follows: in section 2, we give a brief introduction to the model of Arnold et al. (2019, 2020) and describe the assumptions necessary to generate synthetic ion energy spectra. In particular, we explain how the limited field of view of a "real" particle detector is taken into account. Section 3 presents the analysis of synthetic ion energy spectrograms for different plume-plasma interaction scenarios and detector viewing geometries. We consider the same plasma interaction scenarios as Arnold et al. (2019, 2020) to complement the analysis of magnetic field signatures along synthetic and real flyby trajectories presented in these two studies. In particular, we present model results for the expected particle signatures of the plume observed during E26 (Arnold et al., 2019). Section 4 concludes the paper with a summary of our major findings.

2. Model Description

2.1. Hybrid Code Setup

Like Arnold et al. (2019, 2020), we use the hybrid code AIKEF (Müller et al., 2011), which treats ions as (macro) particles and electrons as a massless, charge-neutralizing fluid. Thus, our model is able to describe the flow shear between the magnetospheric plasma and Europa's ionospheric species (plume and exosphere). Blöcker et al. (2016) and Arnold et al. (2019) showed that, to study plume-plasma interactions at Europa, it is essential to use a model that takes into account the ionospheric Hall effect within the plumes. In addition to Europa's plasma environment, AIKEF has already been applied, for example, to analyze flybys through the Enceladus plume (Kriegel et al., 2009, 2011, 2014) and to study induction and plasma interaction signatures at Callisto (Liuzzo et al., 2015, 2016, 2017, 2018).

In this study, we analyze synthetic ion energy spectrograms for three model setups. Within each setup, the magnetospheric upstream parameters and the model of Europa's global atmosphere are kept the same. For each of these three setups, we have carried out multiple simulation runs, placing a local plume source at different locations on Europa's surface. Setups #1 and #2 consist of three runs each, with the plume source located at Europa's south pole and the apices of its leading and trailing hemispheres, respectively. In each model run, only a *single* plume source is considered. For the spectrograms of setups #1 and #2, we use the model configurations described in detail in sections 2 and 3 of Arnold et al. (2020). Setups #1 and #2 differ only in the strength and orientation of the magnetospheric background field $\vec{B}_0$, which also determines the magnetic moment induced in Europa's subsurface ocean. For the third setup, we use the model parameters of Arnold et al. (2019), which correspond to the plasma environment during the Galileo E26 flyby of Europa. In this setup, the location of the plume is chosen in agreement with actual Galileo magnetometer observations from E26.

We use the Cartesian coordinate system EPhiO for our model. In this coordinate system, the x axis is aligned with the corotational plasma flow direction, the y axis points toward Jupiter, the z axis completes the right-handed system, and the origin coincides with Europa's center. Additionally, to describe the location of the plume's footpoint for our different plasma interaction scenarios, we use a spherical coordinate system on Europa's surface. In this system (r, θ, ϕ), r is equal to Europa's radius, the latitude θ is measured from the positive z axis, and ϕ denotes west longitude measured clockwise from the positive y axis.

In all seven model runs presented in this paper (three runs each for setups #1 and #2 and one run for the E26 setup), we apply an asymmetric density profile for Europa's global atmosphere, which we assume to consist of molecular oxygen and which is in agreement with observations (Hall et al., 1995; McGrath et al., 2009). A detailed description of the applied model for Europa's atmospheric density profile can be found in Arnold et al. (2020). All model runs of setups #1 and #2 have already been discussed in Arnold et al. (2020). Therefore, we only provide a brief recap of the upstream parameters. The bulk velocity of the (partially) corotating plasma is set to $u_0 = 100\,\text{km/s}$, which is in agreement with Kivelson et al. (2009) and Bagenal et al. (2015). The number density of the upstream ions is $n = 60 \cdot 10^6\,\text{m}^{-3}$, within the range measured during various Galileo flybys (Kurth et al., 2001; Kivelson et al., 2004). The mass of the singly charged upstream ions is set to $m_i = 18.5\,\text{amu}$, and the ion and electron temperatures read $k_B T_i = k_B T_e = 100\,\text{eV}$ (Kivelson et al., 2004). The plasma parameters for the third setup (conditions during the Galileo E26 flyby) are equal to run #2 of Arnold et al. (2019). The bulk velocity of the upstream plasma is again $u_0 = 100\,\text{km/s}$ along the x axis (Bagenal et al., 2015) and its number density is set to $n = 30 \cdot 10^6\,\text{m}^{-3}$ (Kurth et al., 2001), as observed during the E26 flyby.

The vector of the magnetospheric background field for runs of setup #1 is $\vec{B}_0 = (0, 0, -450)\,\text{nT}$. This field orientation and strength coincide with measurements taken when Europa was located close to the center of Jupiter's magnetospheric plasma sheet (Kivelson et al., 1999). The induced magnetic moment from Europa's subsurface ocean disappears under these conditions, that is, the magnetospheric plasma interacts with the moon's atmosphere/ionosphere alone. In setup #2, we set the vector of the magnetospheric background field to $\vec{B}_0 = (0, -210, -450)\,\text{nT}$. This orientation corresponds to the case when Europa is located near the northern edge of Jupiter's magnetospheric plasma sheet. In this scenario, the induced dipole from Europa's subsurface ocean dominates the plasma interaction. The induced dipole moment points in $(+y)$ direction and its magnitude can be found in Arnold et al. (2020). For the E26 scenario, we use the magnetospheric background field observed during the actual Galileo flyby, $\vec{B}_0 = (-22, 205, -379)\,\text{nT}$ (Kivelson et al., 2009), again yielding a non-vanishing induced dipole moment that is (mostly) antiparallel to the y axis. The parameters for all three setups result in a plasma beta of $\beta \approx 0.01$, an Alfvénic Mach number of $M_A \approx 0.3$, and a magnetosonic Mach number of $M_{MS} \approx 0.3$.

For model setups #1 and #2, we analyzed runs for three plume locations, as provided by Arnold et al. (2020). The footpoint F of the plume is located either at the apex of the trailing hemisphere (upstream "U," in spherical coordinates $(r, \theta_F, \phi_F) = (R_E, 90°, 270°)$), the apex of the leading hemisphere (downstream "D," $(r, \theta_F, \phi_F) = (R_E, 90°, 90°)$), or at Europa's south pole ("S," $(r, \theta_F, \phi_F) = (R_E, 180°, 0°)$). In all runs of setups #1 and #2, the plume axis is oriented perpendicular to Europa's surface. For the E26 setup, the plume observed by Galileo was located in Europa's trailing, southern hemisphere $((r, \theta_F, \phi_F) = (R_E, 140°, 300°))$ and (in contrast to setups #1 and #2) the plume axis is not perpendicular to Europa's surface anymore (see Arnold et al., 2019, for details). The properties of the plume within all three model setups are kept unchanged, with a scale height of $h_p = 200\,\text{km}$, opening angle $h_\theta = 15°$, and surface density $n_{p,0} = 3.9 \cdot 10^{15}\,\text{m}^{-3}$. These values are consistent with the models of Jia et al. (2018) and Arnold et al. (2019, 2020) and result in column densities of the plume similar to those observed by HST (Roth et al., 2014; Sparks et al., 2016).

The extension of the simulation domain is the same as in Arnold et al. (2019, 2020): $-10\,R_E \leq x \leq 20\,R_E$, $-15\,R_E \leq y \leq 15\,R_E$, and $-30\,R_E \leq z \leq -30\,R_E$. The simulation grid contains two refinement levels centered around $(0,0,0)$: the grid resolution is 33 km for $|x, y, z| \leq 1.5\,R_E$, 66 km for $1.5\,R_E < |x, y, z| \leq 3\,R_E$, and 132 km at larger distances. The simulations reach stationarity after about one passage of the plasma flow through the simulation domain.

2.2. Particle Detector Setup

Galileo was equipped with two instrument suites which were able to measure particle energies: the plasma subsystem (PLS) and the energetic particles detector (EPD). The purpose of PLS was to study Jupiter's thermal plasma environment, whereas EPD was designed to measure the high-energy particle populations

within Jupiter's radiation belts. Therefore, PLS covered an energy-per-charge (E/q) range from 0.9 eV to 52 keV and EPD from 20 keV to 55 MeV, respectively (Frank et al., 1992; Paterson et al., 1999). Plume ions are injected into the corotating plasma at energies below 1 eV (e.g., Arnold et al., 2019; Blöcker et al., 2016); therefore, we do not expect them to leave a discernible signature in the data collected by an energetic particle detector. However, we note that a plume source may *indirectly* affect energetic ion observations near Europa by, for example, deflecting the energetic ions through the perturbed fields within the Alfvén winglet (Breer et al., 2019; Huybrighs et al., 2020). Our study focuses on generating synthetic ion energy spectra for the thermal plasma flow near Europa at energies below a few keV.

Due to computational limitations on the number of particles within the hybrid simulation, our model cannot capture the exact details of an actual ion detector that is point-like compared to any length scales of the plasma interaction. However, one limiting factor of both Galileo instruments was the finite viewing angle of the respective detector. Our model allows to explore the influence of a finite viewing angle on ion observations near Europa and on the feasibility to identify local plume sources in ion energy spectra. To create a suitable simulation setup, we have chosen to move a spacecraft along synthetic trajectories through the plume sources described in section 2.1 (see Figures 1a and 1b). The model detector has a viewing angle of 90° and covers the energy range of 0–3,000 eV, thereby capturing the entirety of the (thermal) plasma population within the hybrid simulations.

Similar to the Galileo E12 and E26 flybys (which were the only encounters to detect plume sources at Europa), we have chosen a closest approach altitude of 0.3 R_E for the synthetic trajectories in setups #1 and #2. We also keep the flyby geometries simple, by varying only one coordinate along each trajectory (x for the south polar plume and z for the plumes located at the upstream and downstream apices), in exactly the same way as Arnold et al. (2020). Additionally, we generate a set of synthetic ion energy spectra for the E26 flyby geometry, by analyzing ion energies along a straight line fit through C/A of the E26 encounter (see also Figure 1 in Arnold et al., 2019). The synthetic flyby geometries and the associated plume sources are illustrated in the top row of Figure 1: (red) upstream flyby, plume at Europa's ramside apex, (green) downstream flyby, plume at Europa's wakeside apex, (blue) south polar flyby, plume at Europa's south pole, and (purple) E26 flyby geometry and plume source, as observed by Galileo. The magnetic field perturbations observable along these trajectories are discussed in Arnold et al. (2020) for the first three cases and in Arnold et al. (2019) for E26.

On the length scales of the plasma interaction, a spacecraft has negligible size, and within our hybrid model, it would be completely "buried" within a single cell of the simulation grid. However, such a point-like spacecraft would barely be hit by any macroparticles in the model, thereby drastically blurring the modeled spectrograms and increasing the simulation runtime beyond feasibility. Therefore, to generate meaningful results, we have to artificially increase the "effective size" of the region where the detector is able to collect particles. While this region is much larger than in reality, we still keep its size way below the length scales upon which the fields in Europa's plasma interaction region undergo significant changes. In this way, we ensure that the model detector does not average over structures of different physical origin. As shown in Figure 1c, our model detectors are able to "capture" all particles within a cylindrical tube around each spacecraft trajectory. To study the impact of a finite viewing angle on the modeled spectrograms, each tube is divided into four quarter-cylindrical, wedge-like "subdetectors," the axes of which are aligned with the spacecraft trajectory. The opening angle of each subdetector is 90°. This setup roughly simulates what the Europa Clipper plasma instrument would see during a flyby with fixed orientation of the spacecraft (Grey et al., 2018).

For the plume crossings in setups #1 and #2, this results in a segment facing Europa (therefore facing the plume source), a Europa-averted segment, as well as a Jupiter-facing and Jupiter-averted segment, respectively (see Figure 1c). During E26, the Galileo spacecraft moved mainly in ($+y$) direction. In this case, the four subdetectors used to generate synthetic ion energy spectrograms look in $\pm x$ direction (i.e., toward upstream/downstream) and in $\pm z$ direction (i.e., northward/southward), respectively. The synthetic ion energy spectrograms recorded by *each* of the four "subdetectors" are analyzed in our study.

This study mainly focuses on isolating the role of a finite viewing angle for a low-energy plasma detector on observations of plume-plasma interactions. To facilitate straightforward access to the involved physics, the model spacecraft does *not* rotate as it travels through the hybrid simulation domain, that is, the four quarter-cylindrical detectors have a *fixed* orientation and viewing direction with respect to the EPhiO system
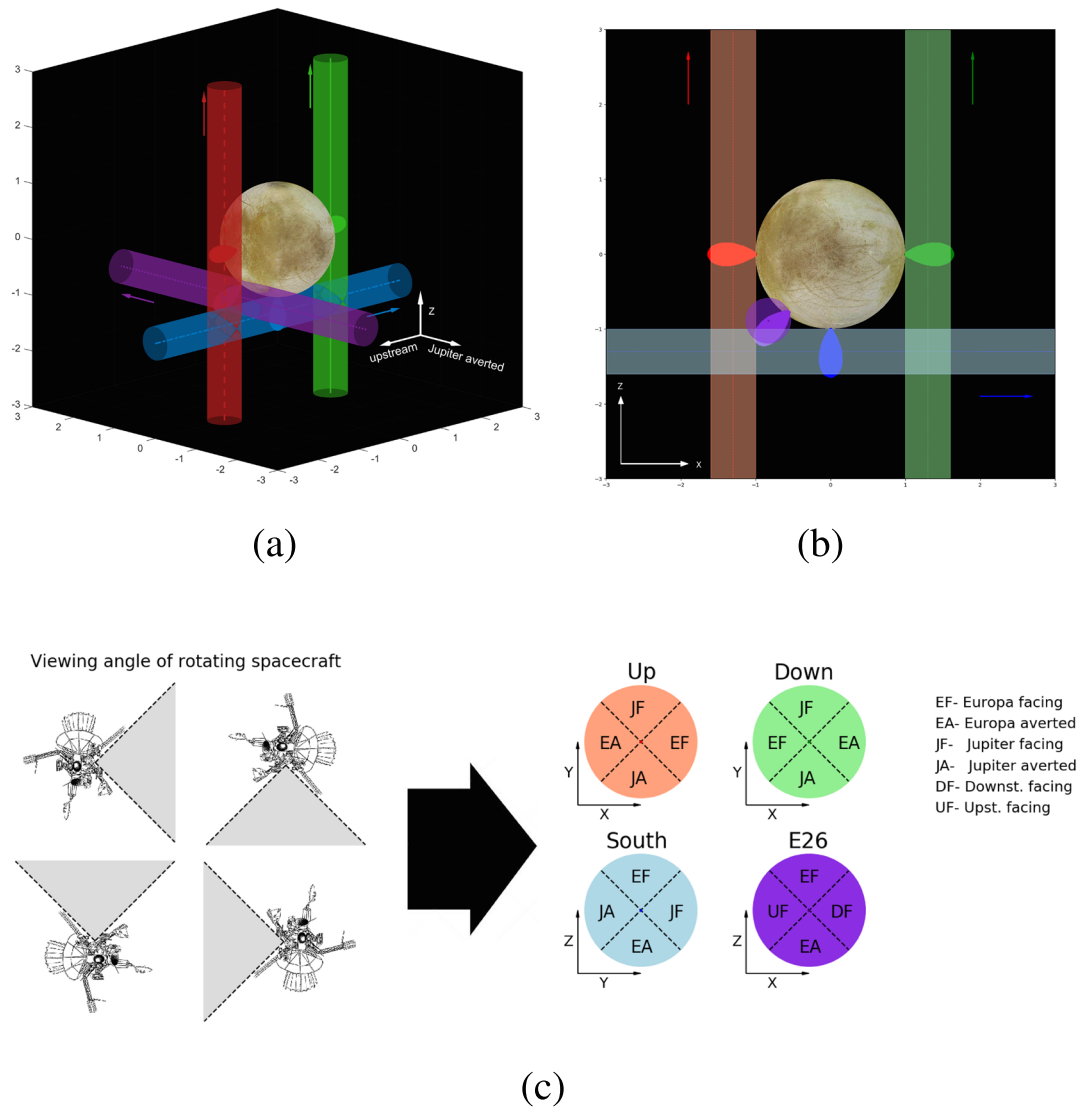
(a)

(b)

(c)

Figure 1. Setup of the synthetic detector geometry used to extract ion energy spectra from the hybrid simulations. In panels (a) and (b), the synthetic trajectories and plume locations considered in this study are displayed. The viewing point in panel (a) is located upstream of Europa and at the Jupiter-averted side, whereas in panel (b), we see Europa from viewing angles $(\theta, \phi) = (180°, 90°)$. The flyby trajectories considered are the same as in Arnold et al. (2019, 2020): the dotted, red line represents a (hypothetical) flyby through a plume located upstream ($x = -1.3\,R_E$, $y = 0$ and z varying), the blue line depicts a crossing of a south polar plume (x varying, $y = 0$, and $z = -1.3\,R_E$), and the green line corresponds to a flyby through a plume located at Europa's leading/downstream apex ($x = 1.3\,R_E$, $y = 0$, and z varying), respectively. During the upstream (red) and downstream (green) flybys, the spacecraft travels northward (toward positive z values), whereas during the south polar flyby, the spacecraft travels toward downstream (x value increasing). Additionally, the violet line corresponds to the E26 flyby geometry, which is approximated by a line fit through the C/A of the E26 encounter ($x = -0.83R_E$, y varying, and $z = -0.89R_E$), see Arnold et al. (2019). The light colors in panels (a) and (b) depict the tube-like regions around the respective trajectories (with radius $0.3\,R_E$) in which particles are collected. The bottom row (c) illustrates the idea behind the detector geometry. In our model, the particle detector is divided into four wedge-like quarter-cylinders, each with an opening angle of 90°. The axis of each quarter-cylinder is aligned with the spacecraft trajectory, that is, the model detectors always "look" in directions perpendicular to the trajectory. On the left side of (c), the resulting viewing angle is presented for different orientations of the spacecraft. On the right side of (c), we show the orientation of the four quarter-cylindrical detectors for each trajectory and their corresponding nomenclature.

and the spacecraft trajectory. During an actual spacecraft flyby through a plume at Europa, the situation would be more complicated (see section 4). However, there are no observed ion energy spectrograms of plume-plasma interactions at Europa available in the literature (neither for E12 nor for E26) to which our model output could be compared at the present time. Therefore, our study rather serves as a "guide" for the interpretation of thermal ion observations from future flybys of Europa.

In our simulation setup, ions are represented by 45 macroparticles per cell and species (collections of particles that have the same charge-to-mass ratio as a real ion) at the highest refinement level (cubes with a length of 33 km). This value is by many orders of magnitude lower than the number of ions populating such a cube in reality. We therefore extend the area of detection to a cylindrical tube of radius $0.3\,R_E$ around each trajectory (see Figures 1a and 1b). We have verified that while reducing the radius of the cylindrical detection region to values below $0.3\,R_E$ does blur the spectrograms, it does *not* add or change any of the physical structures seen. However, only a small fraction of the particles located within the quarter-cylindrical detection segment is actually counted by the respective detector: in order to be registered by a certain detector segment, the velocity vector of a particle must point toward the detector and must be (anti)parallel to the symmetry axis of the respective quarter-cylindrical segment. For example, the velocity vectors $\vec{v} = (v_x, v_y, v_z)$ of particles inside the tube-like region around the upstream flyby trajectory (the red area in Figures 1a and 1b) have to fulfill the following criteria to be detected: $v_y < 0$ for the Jupiter-facing, $v_y > 0$ for the Jupiter-averted, $v_x > 0$ for the Europa-averted, and $v_x < 0$ for the Europa-facing segment, respectively (see Figure 1c). This approach partially takes into account the limitations associated with the finite viewing angle of an actual particle detector: in a real world scenario, the velocity vector of a particle has to be opposite to the temporary viewing direction and location of the detector to enter the device and be registered.

We note that our approach does *not* consider several components of the interaction that the plumes may contribute to: (1) our model does not take into account any interaction between the thermal ions and the neutral gas. However, ion detectors are sensitive to dropouts in the particle signatures that result from locally increased neutral densities (Huybrighs et al., 2020). (2) For some missions, the spacecraft velocity may be sufficient to change the observable energy of the ions by a few eV. This effect would have to be included at the lowest energies considered. However, since we do not attempt to reproduce ion observations from a specific, real-world flyby scenario (with known spacecraft velocity), this slight change in energy is not taken into account by our model. (3) Depending on the configuration of the mission, spacecraft charging may also locally affect the dynamics of the thermal ions.

3. Results

In this section, we discuss the synthetic ion energy spectrograms generated for the two generic plasma interaction setups (#1 and #2) as well as for the E26 flyby. To facilitate the interpretation of the spectrograms, we also display the bulk parameters of the plasma flow. A more detailed discussion of the macroscopic plasma properties (bulk velocity U and the number densities of the three ion species) for setups #1 and #2 can be found in Arnold et al. (2020). The plasma properties for the E26 flyby have been discussed in more detail by Arnold et al. (2019).

The spectrograms presented in this study take into account all three ion species included in the hybrid model (upstream ions O^+, exospheric ions O_2^+, and plume ions H_2O^+, see Arnold et al., 2019, 2020). The upstream plasma properties discussed in section 2.1 result in a drifting Maxwellian distribution centered around an energy of $E = 0.5\,m(O) \cdot (100\,\text{km/s})^2 = 835\,\text{eV}$ with width of $kT = 100\,\text{eV}$, extending symmetrically to both higher and lower energies. This distribution is visible at sufficiently large distances to Europa where the plasma perturbations fade away. The plume ions are inserted with an initial velocity of 0.5 km/s along the plume axis (which is slightly below the escape velocity), that is, their initial energy right after ionization is $E = 0.5\,m(H_2O) \cdot (0.5\,\text{km/s})^2 \approx 0.02\,\text{eV}$.

3.1. Setup #1: Plasma Interaction With a Plume and an Asymmetric Global Atmosphere

In the following, we discuss the ion energy spectrograms obtained for flybys through plumes at three different locations. We again emphasize that a separate simulation run has been carried out for each plume location, that is, there is *no* run that considers all three plumes simultaneously. The model results for the electromagnetic fields in setup #1 are presented by Arnold et al. (2020).

3.1.1. South Polar Plume

In the scenario of a south polar plume, the hybrid model results show the stagnation of the plasma flow (see Figure 2, block "S," panel a) near the symmetric main Alfvén wing, as well as the plume's Alfvén winglet in Europa's southern hemisphere. Since $\vec{B}_0$ is aligned with the $(-z)$ axis, the ions from Europa's global atmosphere escape in a narrow tail, symmetric between the $z > 0$ and $z < 0$ hemispheres (see Figure 2, block "S," panel b). The plume ions, on the other hand, leave Europa in a pick-up tail inclined toward the north, since the $\vec{E} \times \vec{B}$ drift is perpendicular to the draped field lines within the southern wing characteristic (see Figure 2, block "S," panel d).

In Figure 2, block "S," panels (i)–(iv), the ion energy spectra for the flyby through a south polar plume are shown. Approaching the plume from the upstream side ($x < 0$), all four spectrograms display the gradually declining contribution of the unperturbed upstream plasma (drifting Maxwellian centered around 835 eV) to the total particle counts for all four viewing directions of the detector. At $x \approx -2\,R_E$, the spacecraft begins to observe the energy drop of the upstream ion population because of the deceleration of the plasma within the main Alfvén wing. This effect is particularly strong near $x \approx 0\,R_E$, when the spacecraft enters the Alfvén winglet generated by the cold plume plasma (see Figure 2, block "S," panel a). Around this point along the trajectory, the spacecraft also enters the tail of newly generated plume ions. The plume ions form a distinct region of dense, low-energy plasma downstream of $x = 0$ (dark red in all four spectrograms for the southern plume, see Figure 2, block "S," panels i–iv). The spacecraft remains immersed into low-energy plume plasma as it continues to travel toward downstream, until the trajectory leaves the dense center of the inclined tail of plume ions beyond $x > 5\,R_E$. This is particularly well visible in Figure 2, block "S," panel (iii) where the particle energy steadily increases as the spacecraft travels farther downstream and the contribution of the cold plume ions to the total number of counts gradually drops.

The spectrograms observed by a Jupiter-facing (Figure 2, block "S," panel iv) and a Jupiter-averted (Figure 2, block "S," panel ii) detector are nearly identical, since the gyroradii of plume ions ($\approx 10\,$km) in the strong magnetic field near Europa are only a small fraction of moon's radius. However, the most striking result of this run is revealed by comparing the spectrograms in panels (i) (detector pointing toward Europa) and (iii) (detector pointing away from Europa) of Figure 2, block "S": the signature of the plume in the ion energy spectrograms is much more prominent when the detector is directed *away* from the surface of Europa, that is, *away* from the actual location of the plume. Due to the inclination of the magnetic field lines in the southern Alfvén wing, the guiding center trajectories of the drifting plume ions are slightly inclined northward. Therefore, these pick-up ions move *away* from a detector looking toward Europa and *toward* a detector facing the opposite direction.

For a spacecraft trajectory that passes Europa closer than the scale height of a south polar plume, this means that even a weak tilt in the magnetic field near Europa has a discernible effect on the detectability of the plume in thermal ion energy spectrograms. The strongest signal of a south polar plume in ion energy data is expected when the spacecraft actually crosses the plume, but the detector looks *away* from Europa. With increasing Alfvénic Mach number of the upstream flow and thus increasing tilt of the southern wing characteristic against the z axis, this surprising effect will become more pronounced. For a detector looking toward Europa, the tilt in the plume ion trajectories even causes a complete (but very narrow) depletion of the observable ion population immediately downstream of $x = 0$ (see Figure 2, block "S," panel i): the plume ions cannot enter this detector, since their motion is aligned with the viewing direction. Simultaneously, the magnetospheric ions are deflected around the densest region of the plume (Arnold et al., 2020) and cannot reach this detector either.

3.1.2. Upstream Plume

The plasma quantities for a plume located at Europa's upstream apex are nearly symmetric between the $z > 0$ and $z < 0$ half spaces, since the plume axis is aligned with $z = 0$ and the magnetic field points in $(-z)$ direction (see Figure 2, block "U," panels a–d). The perturbations generated by the plume are mainly confined to the upstream region, since newly generated plume ions are immediately picked-up and "rain" back onto Europa's surface (see Figure 2, block "U," panel d, and discussion in Arnold et al., 2019, 2020). Most notably, the plume ions do *not* form a pick-up tail downstream of Europa in this case. The narrow tail formed by ions from the global atmosphere qualitatively resembles the tail formed in the case of a south polar plume, with the slight differences in the electromagnetic field perturbations introducing only very subtle changes to the overall tail structure far downstream of Europa (see Figure 2, block "U," panels b and d).
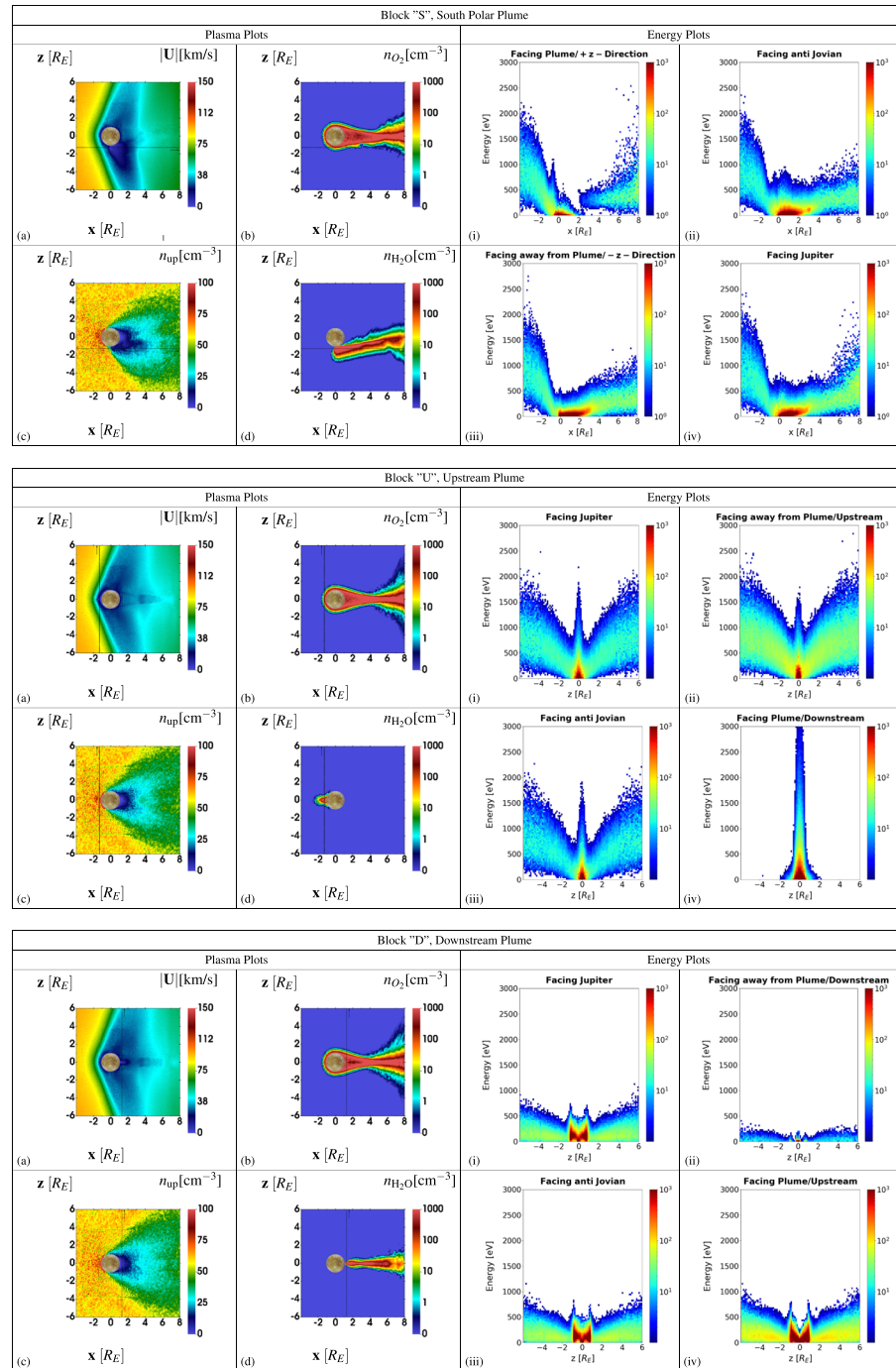
Figure 2. Bulk properties of the plasma flow and synthetic ion energy spectrograms for setup #1. For each plume location on the surface ("S": south polar, "U": upstream, "D": downstream), the three blocks of the figure display, on the left side, (a) the ion bulk velocity, (b) the ion density associated with Europa's global exosphere, (c) the upstream ion density, and (d) the plume ion density in the (x, z) plane of the EPhiO system. The panels on the right side (i–iv) show the modeled ion energy spectrograms for the corresponding spacecraft trajectories and detector orientations from Figure 1. In the spectrograms, the color bar provides the number of counts and energy is given in eV. In block "S," the spacecraft moves along the $(y = 0, z = -1.3R_E)$ line, whereas in block "U," the hypothetical trajectory is located at $(x = -1.3R_E, y = 0)$. In block "D," the spacecraft trajectory is given by $(x = +1.3R_E, y = 0)$.

In the modeled ion energy spectra for a plume located at Europa's upstream apex, the plume generates a distinct, ray-like enhancement in the ion count rates (at low energies of only a few eV) around $x = 0$. This enhancement is much narrower than in the south polar case since the spacecraft only briefly intersects the region populated by cold plume ions. Except for the detector looking toward Europa (see Figure 2, block "U," panel iv), the drifting Maxwellian distribution of the magnetospheric upstream ions is clearly discernible around energies of 835 eV. The "gap" in the upstream ion population is much narrower than in the south polar case because the region populated by plume ions is confined to a narrow "pillar" upstream of Europa (see Figure 2, block "U," panel d). In addition, the trajectory in front of Europa passes the ion deflection region around the Alfvén wings within the interval of $-2R_E \leq z \leq 2R_E$. The plume signal is most clearly visible in the detector facing Europa's surface (see Figure 2, block "U," panel iv), since no upstream plasma enters this detector from the $(-x)$ direction. Also, the scale height of the plume exceeds the scale height of the global atmosphere, that is, only very few pick-up ions from the global atmosphere contribute to the observed signature. The spectrogram recorded by the Europa-facing detector is therefore not "contaminated" by signatures of the other thermal ion species involved in Europa's plasma interaction. This is "convenient," since only a highly sensitive mass spectrometer could discriminate between the water group ions from the plume and oxygen ions from the upstream flow.

The upstream flow directly enters the Europa-averted detector (see Figure 2, block "U," panel ii) and generates a broad signature throughout almost the entire flyby. Since the twisting of the plasma flow direction by the Hall effect within Europa's "main" Alfvén wings (generated by the global exosphere) is rather weak (Arnold et al., 2020; Kivelson et al., 2004; Simon et al., 2011), there is no significant motion of the plasma toward the Jupiter-facing (Figure 2, block "U," panel i) and Jupiter-averted detectors (Figure 2, block "U," panel iii) along a trajectory in the $y = 0$ plane. Upstream particles entering these two detectors are mainly driven by thermal motion. Therefore, the upstream ion counts observed by a detector facing upstream are higher than the counts measured in the other three detector orientations.

Hence, to identify an upstream plume in ion energy spectra without "contamination" by other ion species, a detector looking toward Europa (while remaining outside of the global atmosphere) seems to be the most promising approach. Additionally, we note that the plume location in this run is not too dissimilar from that of the E26 plume. Therefore, these results suggest that, if the PLS detector aboard Galileo had been looking toward Europa, the chances of capturing a signature of the E26 plume would have been high. However, the E26 scenario is still more complicated due to the induced dipole field and the inclination of the upstream field. Details are discussed in section 3.3.

3.1.3. Downstream Plume

Similar to the run with an upstream plume, the Alfvén wings are symmetric between the north and south (see Figure 2, block "D," panel a). No longer being blocked by Europa, the plume forms a narrow pick-up tail (Figure 2, block "D," panel d) that is completely immersed in the "main" pick-up tail emerging from the global ionosphere (Figure 2, block "D," panel b). Since the plume is not directly exposed to the upstream plasma, the plume's signature is nearly invisible in the bulk velocity and the magnetic field (Arnold et al., 2020). The deflection of the plasma flow is mainly determined by the interaction with Europa's global ionosphere, rather than by the plume "hidden" in Europa's wake.

The ion spectra for a flyby through a plume at Europa's downstream apex are nearly devoid of any signatures of the upstream plasma. In Europa's wake, the flow has already been drastically decelerated by mass loading. As can be seen from Figure 2, block "D," panels (i)–(iv), there are practically no plasma particles observed with energies in excess of 500 eV. For a detector facing downstream (Figure 2, block "D," panel ii) no clear signal is visible from any ion population, since all ion species mainly move into the Europa-averted direction. Only the thermal motion of magnetospheric and exospheric plasma can be captured by a detector in this viewing geometry. The other detector geometries show an M-like signature of cold plasma within the moon's geometric plasma shadow ($-1R_E < z < 1R_E$). While the masses of plume ions and exospheric ions are very similar, the M-like signature visible in panels (i), (iii), and (iv) of Figure 2, block "D," is indeed mainly generated by Europa's global exosphere. The two "spikes" of the M feature occur near the points where the spacecraft enters or leaves Europa's geometric plasma shadow. Around these locations, the column density of ionospheric plasma is largest (along straight lines parallel to the x axis), whereas it minimizes in the middle of the M feature around $x = 0$ (see also Figure 1 of Simon, 2015). Since the gyroradii of escaping ions at Europa are small, assuming them to move along straight lines parallel to the x axis is a reasonable approximation, at least in the immediate vicinity of the moon. Therefore, the amount of escaping plasma

"along a line of sight" (parallel to the x axis) is largest at the edges of Europa's geometric plasma shadow and minimizes at its center, thereby generating the M-like feature in our modeled spectrograms. In other words, at the edges of Europa's geometric plasma shadow, escaping ions from the moon's ramside are no longer "blocked" by the solid body, thereby causing a local enhancement in the net outflow.

The fact that the escaping plume ions are unable to generate a third spike in the middle of the M signature suggests that the contribution of these ions is completely "obscured" by pick-up from the global exosphere. However, as will be discussed in the next section, this actually changes when Europa is located away from the center of Jupiter's plasma sheet and the induced dipole field needs to be included.

Like in Arnold et al. (2020), the downstream plume is neither visible in the magnetic field nor in the plasma bulk velocity. The plume is not clearly discernible in the ion energy spectra either. In order to identify the downstream plume in the admixture of ion species in Europa's wake, a high-resolution mass spectrometer would be needed to discriminate between the H_2O (plume), the O (upstream), and the O_2 (ionosphere) species. Judging from magnetic field and ion energy spectrograms only, a spacecraft could indeed cross an active plume at Europa's downstream apex without detecting any discernible signatures of its presence. We also note that mere sputtering of Europa's surface ice releases H_2O molecules as well (e.g., Cassidy et al., 2013). In data from a mass spectrometer, these particles would "compete" with the water molecules associated with an active plume eruption. However, while much lower than the energy of the incident magnetospheric ions, particles emanating from the plume and from surface sputtering would likely still have distinctly different energies.

3.2. Setup #2: Plasma Interaction With an Induced Dipole, a Plume, and an Asymmetric Global Atmosphere

In this setup, the orientation of the magnetic background field is $\vec{B}_0 = (0, -210, -450)$ nT. Due to the non-zero B_y component of the background field, the Alfvén wing characteristics are no longer located in the $z = 0$ plane. The northern wing is inclined toward Jupiter, whereas the southern wing is tilted away from Jupiter by about 25°. Additionally, the cross section of the Alfvén wing is reduced by the presence of an induced dipole (Neubauer, 1999; see Figure 5 of Arnold et al., 2020).

3.2.1. South Polar Plume

The pick-up tails of plume and exospheric ions are rotated out of the (x, z) plane. Therefore, within the (x, z) plane, both tails are visible only in Europa's immediate vicinity (see Figure 3, block "S," panels b and d). The perturbations in the bulk velocity (Figure 3, block "S," panel a) and the upstream plasma density (Figure 3, block "S," panel c) are also much weaker than in a rotated plane $(x, \tilde{z})$ containing the wing characteristics. The model output for the $(x, \tilde{z})$ plane containing the wing characteristics has been discussed in Arnold et al. (2020) (see Figure 5 in that work). Here the results for the (x, z) plane are mainly shown to provide context for the interpretation of the ion energy spectrograms which are calculated along flyby trajectories in that plane.

In the $x < 0$ segments of the ion energy spectra, the upstream ion population is again visible, centered around 835 eV. The population of cold plume ions causes a localized "spike" in all four spectrograms, centered around $x = 0$ (Figure 3, block "S," panels i–iv). However, the spacecraft trajectory remains confined to the (x, z) plane and crosses the plume's pick-up tail only close to Europa (between $x \approx 0 - 1R_E$). A Europa-averted detector shows slightly stronger plume signatures (especially around $x = 1R_E$) than a detector facing Europa, since the drift of the plume ions in the draped magnetic field has a northward component. However, the effect is more subtle than in setup #1, as the spacecraft no longer intersects the "core" of the southern Alfvén wing (see section 3.1.1). In the upstream region ($x \leq 0$), count rates for a detector facing away from Jupiter are higher than for a detector facing Jupiter, whereas downstream of the actual plume crossing ($x \geq 2R_E$), the detector facing Jupiter measures slightly higher count rates. This disparity is due to the plasma deflection around the Alfvén wings (look at Figure 4): at the upstream side of the quasi-cylindrical southern Alfvén wing (which is inclined out of the (x, z) plane away from Jupiter), the flow observable by the spacecraft is diverted toward Jupiter, thereby hitting the Jupiter-averted detector. However, at the downstream side of the Alfvén wing, the flow hitting the spacecraft is deflected away from Jupiter and therefore mainly enters the Jupiter-facing detector. This upstream-downstream asymmetry did not occur in setup #1, where $\vec{B}_0$ points in $(-z)$ direction and the flow deflection disappears near the $y = 0$ plane (since the rotation of the fields in the main Alfvén wings due to the Hall effect is rather weak, see Arnold et al., 2020; Kivelson et al., 2004; Simon et al., 2011). In the immediate vicinity of Europa's south pole, the deflection of the magnetospheric ions
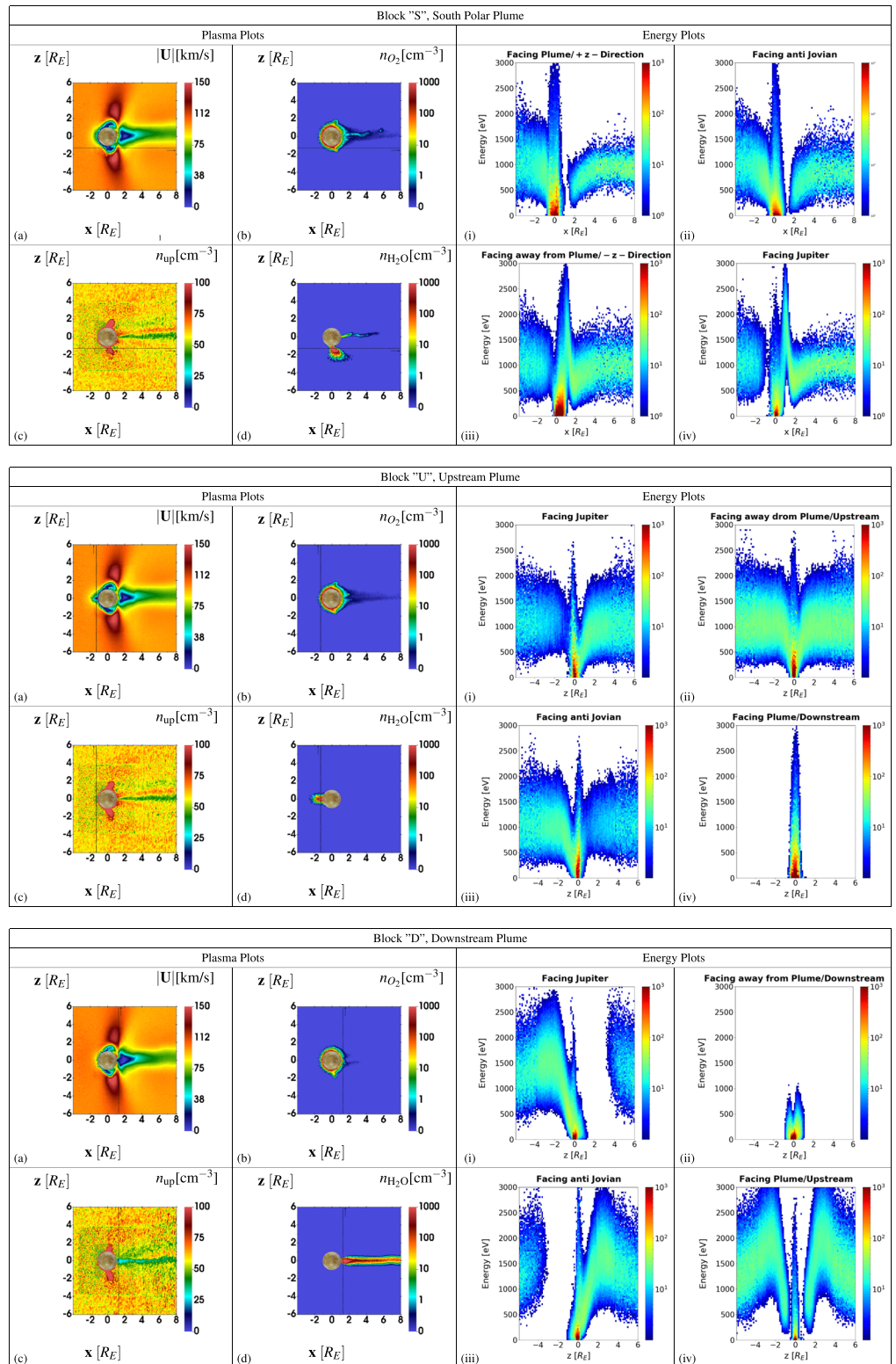
Figure 3. Bulk properties of the plasma flow and synthetic ion energy spectrograms for setup #2. The layout of the figure is identical to that of Figure 2. In block "S," the spacecraft moves along the $(y = 0, z = -1.3R_E)$ line, whereas in block "U," the hypothetical trajectory is located at $(x = -1.3R_E, y = 0)$. In block "D," the spacecraft trajectory is given by $(x = +1.3R_E, y = 0)$.
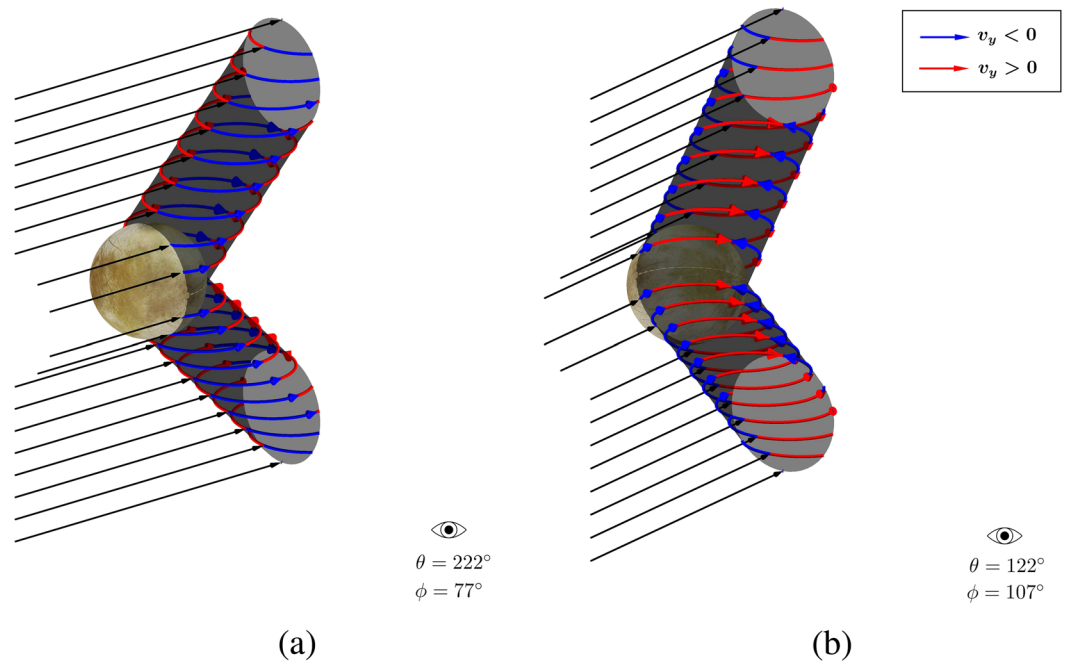
Figure 4. Deflection of the incident magnetospheric plasma around Europa's tilted Alfvén wings. The deflection of the upstream flow (which is aligned with the $+x$ axis) generates alternating regions with a velocity component toward Jupiter ($v_y > 0$, red) or away from Jupiter ($v_y < 0$, blue). (a) Side view from upstream and (b) view from downstream.

around the "core" of the plume, combined with the (almost) unidirectional motion of the plume particles, again causes highly localized gaps in the spectrograms observable by several detectors (see Figure 3, block "S", panels i, ii, and iv).

3.2.2. Upstream Plume

Within the (x, z) plane, the plume is barely visible in macroscopic parameters of the incident magnetospheric plasma for the south polar case, but when located upstream, it causes a distinct drop in the plasma bulk velocity around $x = -1\,R_E$ (see Figure 3, block "U," panel a). As suggested by Arnold et al. (2020), the plasma bulk speed is the only macroscopic quantity that contains discernible plume signatures in this case.

The most suitable approach to identify an upstream plume in particle data is again with a detector pointed toward Europa, since no upstream plasma flow moves in that direction. The spectrogram of Figure 3, block "U," panel (iv), is therefore not "contaminated" by the contribution of the magnetospheric plasma. The spectra for the other three detector orientations (toward upstream, toward Jupiter, and away from Jupiter) are qualitatively similar to the preceding case where Europa was located in the center of Jupiter's plasma sheet and no induced dipole was present (see section 3.1.2). In particular, the spectrogram acquired by a detector looking toward upstream (Figure 3, block "U," panel ii) is nearly identical to the preceding case. Since the x component of an individual ion's velocity alone determines whether it is "seen" by this model detector, the shape of the spectrogram is not affected by the deflection around the Alfvén wing in the ($\pm y$) direction.

However, the spectrograms recorded by the Jupiter-facing and Jupiter-averted detectors now exhibit a north–south asymmetry caused by the inclination of the Alfvén wings and the location of the trajectory upstream of Europa (see Figure 4): in the southern hemisphere, the Alfvén wing is inclined in ($-y$) direction. Therefore, the spacecraft encounters the region where the plasma is deflected toward Jupiter around the southern Alfvén wing. In the northern hemisphere, the Alfvén wing is inclined toward Jupiter and the spacecraft therefore encounters a region where the flow is deflected away from the planet (see also Figure 4 and Figure 21.2 in Kivelson et al., 2004). Hence, a detector facing Jupiter (Figure 3, block "U," panel i) measures increased count rates in Europa's northern hemisphere (where more ions move toward the detector) and reduced count rates in Europa's southern hemisphere. For the detector looking away from Jupiter (Figure 3, block "U," panel iii), the geometry is reversed. However, these deflection patterns do not contain any clearly discernible signature of the Alfvén winglet associated with the plume and can readily be explained through

deflection around the "main" Alfvén wing, generated by the interaction with the global ionosphere (Paterson et al., 1999). For this reason, a "spike" of cold plume plasma near $x = 0$ is indicative of a plume crossing in Europa's upstream hemisphere, but the accompanying deflection features are not specific to the presence of a plume.

3.2.3. Downstream Plume

The thermal plasma parameters are similar to the case with a plume located at Europa's upstream apex (see Figure 3, block "D," panels a–d). The most remarkable feature is that—despite the inclination of the upstream magnetic field—the pick-up tail formed by the plume ions is still oriented along the x axis. On the other hand, the tail formed by ions from the global ionosphere is again rotated out of the (x, z) plane. There is only weak plume-plasma interaction visible in the plasma bulk velocity, since the plume is "shielded" by the solid body of Europa. Pick-up of newly generated plume ions is weakest in this configuration, since the incident plasma is largely deflected around Europa.

In the previous setup (section 3.1.3), without an induced dipole, the downstream plume did not generate a discernible spike in the ion energy spectra, either because the particle production rates were too low or the acceleration due to pick-up was too weak. However, when the dipole is included, the plume generates a distinct spike during the crossing, independent of the detector orientation. For a detector facing the plume, we now see three distinct peaks in the ion energy spectrogram (Figure 3, block "D," panel iv), two of them at the outer edges of Europa's geometric plasma shadow and the third one in its center, coinciding with the position of the plume. Hence, in contrast to the preceding scenario, the plume is now able to superimpose a third, central peak on the initially M-like structure associated with ion pick-up from Europa's global ionosphere (see section 3.1.3). This time, the ion energies are much higher than in the scenario without an induced dipole. The detector facing downstream also detects a highly localized population of cold particles within the bounds of Europa's geometric plasma shadow (see Figure 3, block "D," panel ii). Due to the inclination of the Alfvén wings, Europa's wake in the (x, z) plane is not completely shielded from the upstream plasma anymore. Therefore, this signature corresponds mainly to the thermal motion of slow plasma antiparallel to the bulk flow (see Figure 3, block "D," panel iv).

Similar to the flyby through the upstream plume, the Jupiter-facing and Jupiter-averted detectors display intense signatures of the flow deflection around the tilted "main" Alfvén wing and the associated north–south asymmetry (see Figure 4). The deflected ions start to resume motion in $(+x)$ direction downstream of the Alfvén wing tubes. Therefore, the flow is deflected toward Jupiter in Europa's northern hemisphere, whereas the magnetospheric ions move away from Jupiter in Europa's southern hemisphere. For this reason, the Jupiter-averted detector registers increased particle counts in Europa's northern hemisphere, whereas its spectrogram displays a prominent gap in the southern hemisphere. The opposite can be seen in the data from the Jupiter-facing detector. Since the perturbations associated with Europa's main Alfvén wing are way more intense at the moon's wakeside than along an upstream flyby trajectory (see Arnold et al., 2020, Figure 5, panels a–c), the dips and enhancement signatures in these spectra are much more prominent than in case of an upstream plume.

Overall, in the scenario where Europa is located outside of Jupiter's plasma sheet, the deflection signatures around the main Alfvén wings make a significant contribution to the particle flow into the detector. These signatures dominate the particle spectra and can severely complicate the identification of plume signatures in spacecraft data.

3.3. Plasma Interaction During the Galileo E26 Flyby

Magnetic field and energetic proton data from the E26 flyby are indicative of a plume crossing in Europa's southern trailing hemisphere (Arnold et al., 2019; Huybrighs et al., 2020). For simplicity, the flyby trajectory in our model setup is a straight line through the point of closest approach of E26 at $x = -0.83R_E$, $z = -0.89R_E$, that is, south of Europa's equator. The spacecraft moved in $(+y)$ direction (i.e., toward Jupiter) and intersected the cylinder $\sqrt{y^2 + z^2} = R_E$, thereby penetrating "deeper" into Europa's main Alfvén wing than during the generic cases in sections 3.1 and 3.2. The orientation of the magnetic background field is $\vec{B}_0 = (-22, 205, -379)$ nT, leading to Alfvén wing characteristics which are again inclined against the $z = 0$ plane. To identify the contribution of plume ions to the modeled ion energy spectra, we present results for two runs: one run with a plume and a "baseline scenario" without a plume. Results for both scenarios are shown in Figure 5. The parameters of the incident magnetospheric flow and Europa's global exosphere are
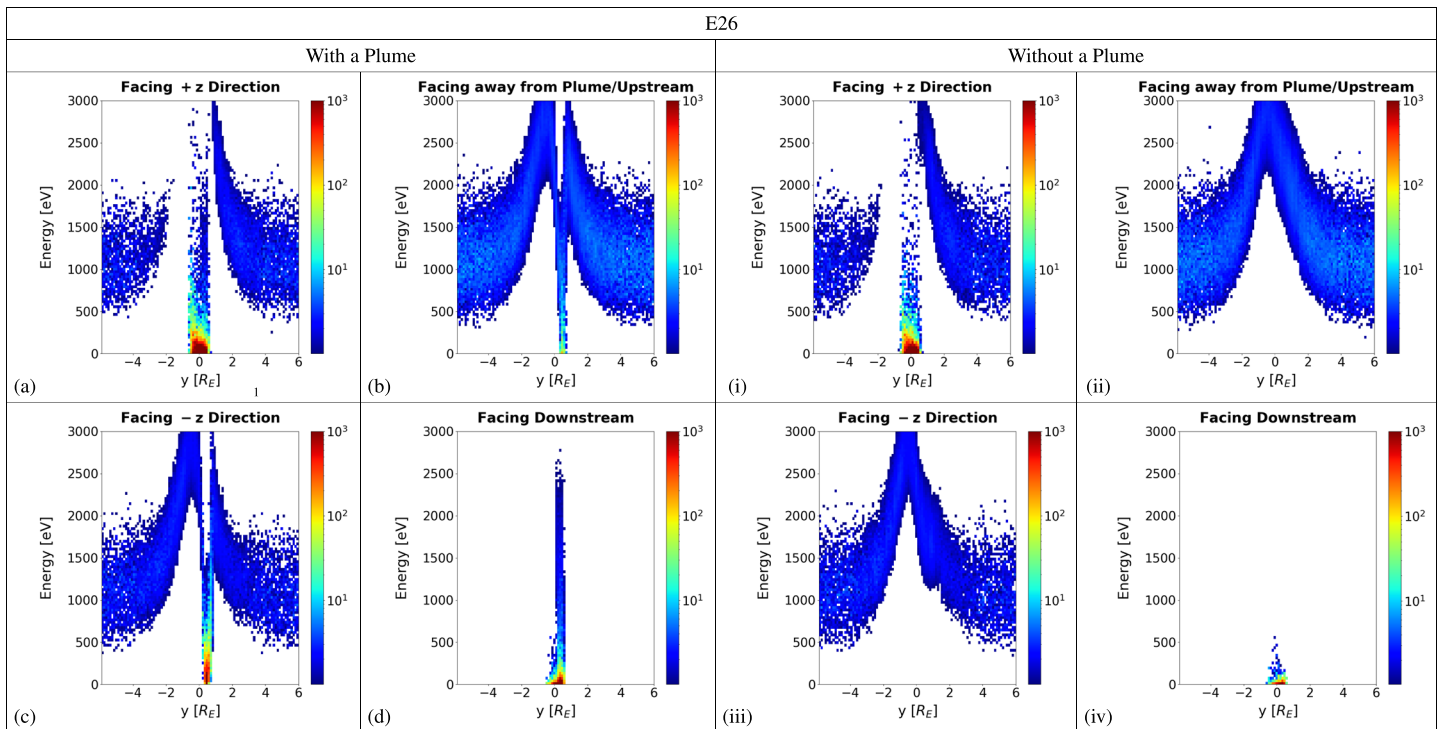
Figure 5. Synthetic ion energy spectrograms, as observable for different viewing directions of a particle detector during the Galileo E26 flyby of Europa. Left block (a–d): with the plume included; right block (i–iv): "baseline run" without the plume.

the same in both runs. The model results for the electromagnetic fields for both setups can be found in Arnold et al. (2019).

The spectrogram recorded by a detector looking toward Europa in $(+x)$ direction (toward downstream, see Figure 5d) contains a clearly discernible signature of the plume, since this detector does not record any magnetospheric upstream particles (similar to Figures 2 and 3, block "U," panels iv). However, for this detector orientation, the difference between a run with (Figure 5d) and without a plume (Figure 5iv) is rather quantitative than qualitative. Without a plume, the spacecraft still observes a localized enhancement in the spectrogram when it "scratches" the outer regions of Europa's atmosphere around closest approach. The intensity of this peak is amplified by more than an order of magnitude (at energies below 500 eV) when a plume is included. However, to infer the presence of a plume, one would need a very accurate model of Europa's global atmosphere at the time of E26, since the plume does not generate any qualitatively new signatures in the "downstream" spectrogram.

In the spectrogram from a detector looking away from the plume in $(-x)$ direction (i.e., toward upstream, see Figure 5b), the upstream ion population is visible outside of the interaction region. Around closest approach, upstream ions are accelerated and deflected at the flanks of Europa's southern Alfvén wing. Count rates are therefore shifted toward higher energies (up until $\approx 3,000$ eV). When a plume is included, a characteristic dip is carved into the "bell-like" acceleration feature in the spectrogram, since newly generated plume ions have not yet obtained a significant velocity at the altitude of the flyby. Surprisingly, the detector looking toward upstream (away from Europa) obtains a more clearly visible plume signature than the detector looking toward downstream (toward Europa). The reason for this is that around closest approach of E26, the spacecraft was immersed in the population of cold plume ions while still remaining "far enough upstream" to detect the deflection of the incident magnetospheric ions by the Alfvén wing (let). Due to its small scale height (compared to that of the plume), ions from Europa's global exosphere do not appear in either of the two spectrograms (Figures 5b and 5ii) for this viewing direction. The cold plume ion population is therefore clearly discernible over the "background" of warm, deflected magnetospheric flow. These ions have just been picked up, thereby moving back toward Europa. A detector looking southward (in $-z$ direction, see Figure 5c) observes almost the same features, since the detector is oriented away from the plume as well and is also able to capture a decent portion of the upstream particles.
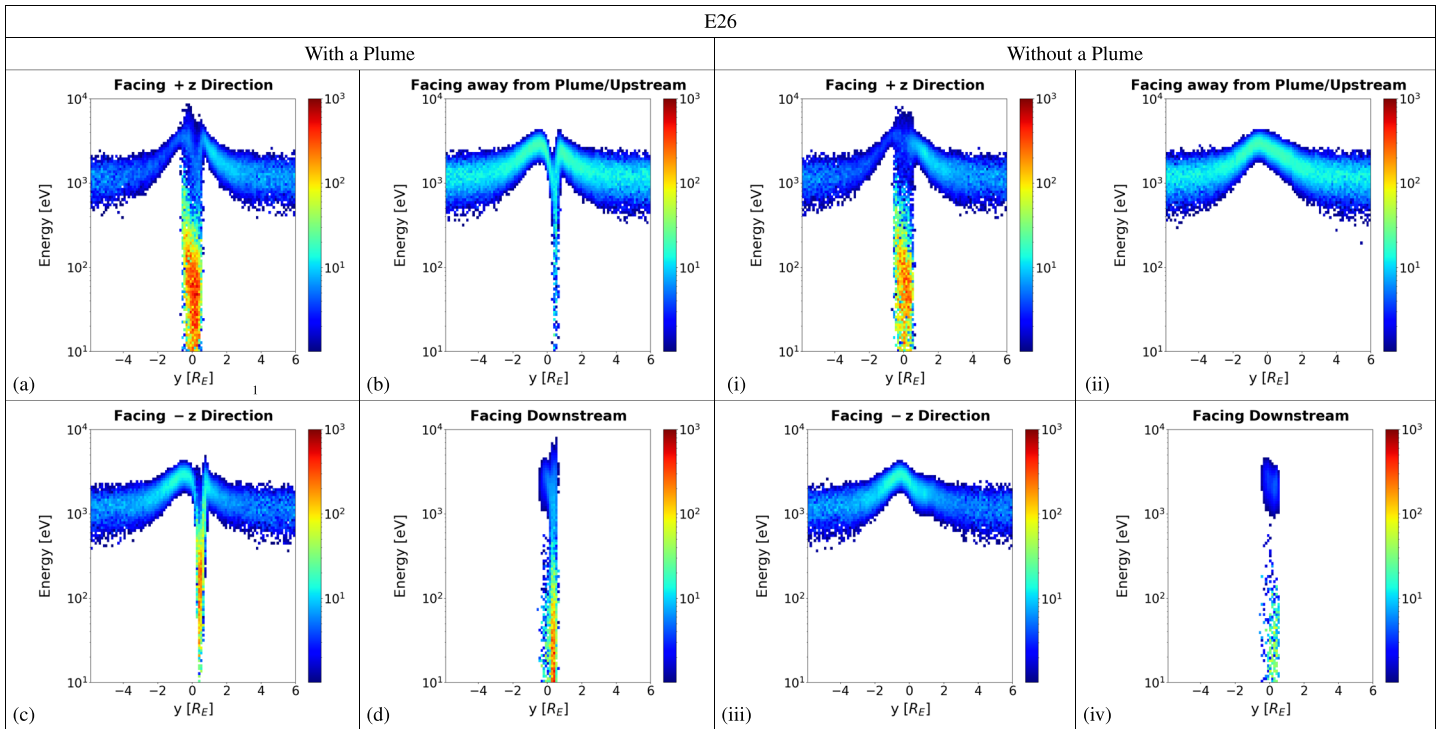
Figure 6. Synthetic ion energy spectrograms for the E26 flyby. The model output shown is the same as in Figure 5. However, here the spectrograms are plotted on a logarithmic energy scale.

If the detector faces into the $(+z)$ direction (northward, see Figure 5a), its field of view is partially "obscured" by Europa's solid body (see Figure 1b, violet cylinder). In the run without a plume (Figure 5i), the model reveals a highly asymmetric deflection feature: two uneven outer flanks with peak energies above 2,000 eV, caused by the deflection of the upstream flow around Europa's inclined southern Alfvén wing, and a dip in between, generated by Europa's cold exospheric ions. When a plume is included, the deflection pattern barely changes. Thus, for a detector looking in $(+z)$ direction, the differences between both runs are rather quantitative than qualitative and not sufficient to obtain clear evidence for the presence of the plume.

In conclusion, a detector facing toward upstream or southward would have had the highest chances to identify the E26 plume in thermal plasma data. Only in these spectrograms, the presence of the plume causes qualitative differences to a scenario that considers only Europa's global atmosphere, but no plume. This confirms our earlier finding that a detector looking toward Europa does not necessarily have the highest chances of unambiguously identifying a plume source on the moon's surface.

In practical applications, ion energy spectrograms are often plotted with a logarithmic energy axis. To illustrate the impact of such a rebinning on the shape of the spectrograms, Figure 6 displays the modeled spectrograms for E26, but with a logarithmic energy axis. As can be seen, logarithmic energy binning provides better resolution of the low-energy plume ion population. However, this approach also drastically attenuates the deflection features visible in the incident magnetospheric ion population. In our model scenarios, the deflection of the upstream particles often made the strongest contribution to the plasma interaction signatures associated with a plume.

4. Summary and Concluding Remarks

Using the output of a hybrid model (Arnold et al., 2019, 2020), we have generated synthetic energy spectrograms of the thermal ion population observable in the vicinity of plumes at various locations on Europa's surface. In this way, we have assessed the influence of the local electromagnetic field perturbations and the viewing geometry on the detectability of potential plume signatures in Europa's thermal plasma environment by a spacecraft.

Our results show that even in the immediate vicinity of Europa, flow deflection by the moon's Alfvén wings has a drastic influence on the observability of pick-up ions from a local plume source. For instance, the pick-up tail formed by a plume at Europa's south pole is slightly "lifted" northward by the draped magnetic field in the moon's southern Alfvén wing. In this process, the plume ions' drift velocity gains a component *toward* Europa, that is, a detector looking *away* from the moon is most suitable to observe this newly generated ion population. In addition, the Alfvén winglet generated by a plume locally amplifies the deflection of the incident magnetospheric plasma around the obstacle, thereby generating an indirect signature of the plume in the ion energy spectrograms. However, in order to isolate the additional deflection of the upstream ions caused by the Alfvén winglet, a reference spectrogram would be required for an interaction scenario that does *not* consider the plume source.

Depending on the viewing direction of a thermal particle detector, the ion population associated with a plume may also be partially or completely obscured by the incident magnetospheric ions. While this is evident when the detector is oriented toward upstream, the strong deflection of the incident magnetospheric flow around Europa's Alfvén wings may also obstruct the plume ions in the recording of a detector that looks, for example, toward or away from Jupiter.

Overall, our results suggest that thermal ion energy spectrograms provide a valuable diagnostic tool to support the identification of local plume sources at Europa through in situ observations. However, only for very few specific flyby geometries and plume locations, the signatures in these spectrograms are "sufficiently unique" to be directly associated with the presence of a plume of water vapor. Also, the spectrograms presented in this study have been generated under the assumption that the viewing direction of the particle detector remains fixed during a close flyby. In reality, however, the detector orientation will continuously change throughout the flyby due to the inherent rotation of the spacecraft and the detector itself. Thus, the actual energy spectrograms observed during a Europa flyby will consist of a sequence of "vertical slices" through the time series obtained for fixed viewing directions in this study. In some cases, the signatures associated with a plume crossing are particularly narrow, such as the highly localized enhancement in ion counts generated by a source at Europa's wakeside apex. In such a case, an unfavorable momentary viewing geometry will cause the plasma detector to completely miss any potential signatures of the plume passage. The detectability of such localized plume signatures ultimately depends on the rotation period of the spacecraft, compared to the time it needs to travel through the perturbations caused by the plume. Also, changes in the upstream conditions throughout the duration of a flyby could add dynamic features to the spectrograms which may further shroud the signatures associated with a plume.

Our study reveals that plumes can often be identified in the spectrograms in an indirect way, that is, through the pronounced "gaps" that they carve into the distribution of the incident magnetospheric ions (which have energies on the order of 1 keV). Taking into account the non-zero velocity of the spacecraft would mainly shift the energy range of the cold plume ions in the spectrograms by a few eV. However, the energy of the plume ions would still be much lower than that of the magnetospheric ions. Thus, in a real-world scenario, the general shape of the spectrograms would remain very similar to the results shown here. Overall, the identification of plumes through the perturbations they leave in particle and field data will always require to take into account information on multiple components of Europa's plasma interaction (e.g., thermal ions, energetic ions, magnetic field).

Data Availability Statement

Results from the AIKEF hybrid model can be downloaded and accessed online (http://doi.org/10.5281/zenodo.3385994 and http://doi.org/10.5281/zenodo.3902730).

References

Arnold, H., Liuzzo, L., & Simon, S. (2019). Magnetic signatures of a plume at Europa during the Galileo E26 flyby. *Geophysical Research Letters*, *46*, 1149–1157. https://doi.org/10.1029/2018GL081544

Arnold, H., Liuzzo, L., & Simon, S. (2020). Plasma interaction signatures of plumes at Europa. *Journal of Geophysical Research: Space Physics*, *125*, e2019JA027346. https://doi.org/10.1029/2019JA027346

Bagenal, F., Sidrow, E., Wilson, R. J., Cassidy, T. A., Dols, V., Crary, F. J., et al. (2015). Plasma conditions at Europa's orbit. *Icarus*, *261*, 1–13. https://doi.org/10.1016/j.icarus.2015.07.036

Blöcker, A., Saur, J., & Roth, L. (2016). Europa's plasma interaction with an inhomogeneous atmosphere: Development of Alfvén winglets within the Alfvén wings. *Journal of Geophysical Research: Space Physics*, *121*, 9794–9828. https://doi.org/10.1002/2016JA022479

Breer, B. R., Liuzzo, L., Arnold, H., Andersson, P. N., & Simon, S. (2019). Energetic ion dynamics in the perturbed electromagnetic fields near Europa. *Journal of Geophysical Research: Space Physics*, *124*, 7592–7613. https://doi.org/10.1029/2019JA027147

Burger, M. H., & Johnson, R. E. (2004). Europa's neutral cloud: Morphology and comparisons to Io. *Icarus*, *171*, 557–560. https://doi.org/10.1016/j.icarus.2004.06.014

Cassidy, T. A., Paranicas, C. P., Shirley, J. H., Dalton III, J. B., Teolis, B. D., Johnson, R. E., et al. (2013). Magnetospheric ion sputtering and water ice grain size at Europa. *Planetary and Space Science*, *77*, 64–73. https://doi.org/10.1016/j.pss.2012.07.008

Cooper, J. F., Johnson, R. E., Mauk, B. H., Garrett, H. B., & Gehrels, N. (2001). Energetic ion and electron irradiation of the icy galilean satellites. *Icarus*, *149*(1), 133–159. https://doi.org/10.1006/icar.2000.6498

Frank, L. A., Ackerson, K. L., Lee, J. A., English, M. R., & Pickett, G. L. (1992). The plasma instrumentation for the Galileo mission. *Space Science Reviews*, *60*, 1572–9672. https://doi.org/10.1007/BF00216858

Giono, G., Roth, L., Ivchenko, N., Saur, J., Retherford, K., Schlegel, S., et al. (2020). An analysis of the statistics and systematics of limb anomaly detections in HST/STIS transit images of Europa. *The Astronomical Journal*, *159*(4), 155. https://doi.org/10.3847/1538‐3881/ab7454

Grey, M., Westlake, J., Liang, S., Hohlfeld, E., Crew, A., & McNutt, R. (2018). Europa pims prototype faraday cup development. In *2018 IEEE Aerospace Conference*, pp. 1–15.

Hall, D. T., Strobel, D. F., Feldman, P. D., McGrath, M. A., & Weaver, H. A. (1995). Detection of an oxygen atmosphere on Jupiter's moon Europa. *Nature*, *373*, 677–679. https://doi.org/10.1038/373677a0

Hand, K. P., & Chyba, C. F. (2007). Empirical constraints on the salinity of the Europan ocean and implications for a thin ice shell. *Icarus*, *189*(2), 424–438. https://doi.org/10.1016/j.icarus.2007.02.002

Hussmann, H., Spohn, T., & Wieczerkowski, K. (2002). Thermal equilibrium states of Europa's ice shell: Implications for internal ocean thickness and surface heat flow. *Icarus*, *156*(1), 143–151. https://doi.org/10.1006/icar.2001.6776

Huybrighs, H. L. F., Roussos, E., Blocker, A., Krupp, N., Futaana, Y., Barabash, S., et al. (2020). An active plume eruption on Europa during Galileo flyby e26 as indicated by energetic proton depletions. *Geophysical Research Letters*, *47*, e2020GL087806. https://doi.org/10.1029/2020GL087806

Jia, X., Kivelson, M. G., Khurana, K. K., & Kurth, W. S. (2018). Evidence of a plume on Europa from Galileo magnetic and plasma wave signatures. *Nature Astronomy*, *2*, 459–464. https://doi.org/10.1038/s41550-018-0450-z

Khurana, K. K., Kivelson, M. G., Stevenson, D. J., Schubert, G., Russell, C. T., Walker, R. J., & Polanskey, C. (1998). Induced magnetic fields as evidence for subsurface oceans in Europa and Callisto. *Nature*, *395*(6704), 777–780. https://doi.org/10.1038/27394

Kivelson, M. G., Bagenal, F., Kurth, W. S., Neubauer, F. M., Paranicas, C., & Saur, J. (2004). Magnetospheric interactions with satellites. In F. Bagenal, T. E. Dowling, & W. B. McKinnon (Eds.), *Jupiter. The planet, satellites and magnetosphere* (pp. 513–536). Cambridge: Cambridge Univ. Press.

Kivelson, M. G., Khurana, K. K., Russell, C. T., Volwerk, M., Walker, R. J., & Zimmer, C. (2000). Galileo magnetometer measurements: A stronger case for a subsurface ocean at Europa. *Science*, *289*, 1340–1343. https://doi.org/10.1126/science.289.5483.1340

Kivelson, M. G., Khurana, K. K., Stevenson, D. J., Bennett, L., Joy, S., Russell, C. T., et al. (1999). Europa and Callisto: Induced or intrinsic fields in a periodically varying plasma environment. *Journal of Geophysical Research*, *104*(A3), 4609–4626. https://doi.org/10.1029/1998JA900095

Kivelson, M. G., Khurana, K. K., & Volwerk, M. (2009). Europa's interaction with the Jovian magnetosphere. In R. T. Pappalardo, W. B. McKinnon, K. K. Khurana, R. Dotson, et al. (Eds.), *Europa* (pp. 545), The University of Arizona space science series. Tucson: University of Arizona Press.

Kriegel, H., Simon, S., Meier, P., Motschmann, U., Saur, J., Wennmacher, A., et al. (2014). Ion densities and magnetic signatures of dust pick-up at Enceladus. *Journal of Geophysical Research: Space Physics*, *119*, 2740–2774. https://doi.org/10.1002/2013JA019440

Kriegel, H., Simon, S., Motschmann, U., Saur, J., Neubauer, F., Persoon, A., et al. (2011). Influence of negatively charged plume grains on the structure of Enceladus Alfvén wings: Hybrid simulations versus Cassini magnetometer data. *Journal of Geophysical Research*, *116*, A10223. https://doi.org/10.1029/2011JA016842

Kriegel, H., Simon, S., Müller, J., Motschmann, U., Saur, J., Glassmeier, K.-H., & Dougherty, M. (2009). The plasma interaction of Enceladus: 3d hybrid simulations and comparison with Cassini mag data. *Planetary and Space Science*, *57*(14), 2113–2122. https://doi.org/10.1016/j.pss.2009.09.025

Kurth, W., Gurnett, D., Persoon, A., Roux, A., Bolton, S., & Alexander, C. (2001). The plasma wave environment of Europa. *Planetary and Space Science*, *49*(3), 345–363. magnetospheres of the Outer Planets (Part I).

Liuzzo, L., Feyerabend, M., Simon, S., & Motschmann, U. (2015). The impact of Callisto's atmosphere on its plasma interaction with the Jovian magnetosphere. *Journal of Geophysical Research: Space Physics*, *120*, 9401–9427. https://doi.org/10.1002/2015JA021792

Liuzzo, L., Simon, S., & Feyerabend, M. (2018). Observability of Callisto's inductive signature during the JUpiter ICy moons Explorer mission. *Journal of Geophysical Research: Space Physics*, *123*, 9045–9054. https://doi.org/10.1029/2018JA025951

Liuzzo, L., Simon, S., Feyerabend, M., & Motschmann, U. (2016). Disentangling plasma interaction and induction signatures at Callisto: The Galileo C10 flyby. *Journal of Geophysical Research: Space Physics*, *121*, 8677–8694. https://doi.org/10.1002/2016JA023236

Liuzzo, L., Simon, S., Feyerabend, M., & Motschmann, U. (2017). Magnetic signatures of plasma interaction and induction at callisto: The Galileo c21, c22, c23, and c30 flybys. *Journal of Geophysical Research: Space Physics*, *122*, 7364–7386. https://doi.org/10.1002/2017JA024303

McGrath, M. A., Hansen, C. J., & Hendrix, A. R. (2009). Observations of Europa's tenuous atmosphere. In R. T. Pappalardo, W. B. McKinnon, K. K. Khurana, R. Dotson, et al. (Eds.), *Europa* (pp. 485), The University of Arizona space science series. Tucson: University of Arizona Press.

Müller, J., Simon, S., Motschmann, U., Schüle, J., Glassmeier, K., & Pringle, G. J. (2011). A.I.K.E.F.: Adaptive hybrid model for space plasma simulations. *Computer Physics Communications*, *182*(4), 946–966. https://doi.org/10.1016/j.cpc.2010.12.033

Neubauer, F. M. (1980). Nonlinear standing Alfven wave current system at Io—Theory. *Journal of Geophysical Research*, *85*, 1171–1178. https://doi.org/10.1029/JA085iA03p01171

Neubauer, F. M. (1998). The sub-Alfvénic interaction of the Galilean satellites with the Jovian magnetosphere. *Journal of Geophysical Research*, *103*, 19,843–19,866. https://doi.org/10.1029/97JE03370

Neubauer, F. M. (1999). Alfvén wings and electromagnetic induction in the interiors: Europa and Callisto. *Journal of Geophysical Research*, *104*, 28,671–28,684. https://doi.org/10.1029/1999JA900217

Paganini, L., Villanueva, G. L., Roth, L., Mandell, A. M., Hurford, T. A., Retherford, K. D., & Mumma, M. J. (2019). A measurement of water vapour amid a largely quiescent environment on Europa. *Nature Astronomy*, *4*, 1–7. https://doi.org/10.1038/s41550-019-0933-6

Paterson, W. R., Frank, L. A., & Ackerson, K. L. (1999). Galileo plasma observations at Europa: Ion energy spectra and moments. *Journal of Geophysical Research*, *104*(A10), 22,779–22,791. https://doi.org/10.1029/1999JA900191

Pospieszalska, M. K., & Johnson, R. E. (1989). Magnetospheric ion bombardment profiles of satellites—Europa and Dione. *Icarus*, *78*, 1–13. https://doi.org/10.1016/0019-1035(89)90065-1

Roth, L., Saur, J., Retherford, K. D., Strobel, D. F., Feldman, P. D., McGrath, M. A., & Nimmo, F. (2014). Transient water vapor at Europa's south pole. *Science*, *343*(6167), 171–174. https://doi.org/10.1126/science.1247051

Roth, L., Saur, J., Retherford, K. D., Strobel, D. F., Feldman, P. D., McGrath, M. A., et al. (2016). Europa's far ultraviolet oxygen aurora from a comprehensive set of HST observations. *Journal of Geophysical Research: Space Physics*, *121*, 2143–2170. https://doi.org/10.1002/2015JA022073

Saur, J., Neubauer, F. M., Strobel, D. F., & Summers, M. E. (1999). Three-dimensional plasma simulation of Io's interaction with the Io plasma torus: Asymmetric plasma flow. *Journal of Geophysical Research*, *104*(A11), 25,105–25,126. https://doi.org/10.1029/1999JA900304

Schenk, P. M. (2002). Thickness constraints on the icy shells of the Galilean satellites from a comparison of crater shapes. *Nature*, *417*, 419–421.

Simon, S. (2015). An analytical model of sub-Alfvénic moon-plasma interactions with application to the hemisphere coupling effect. *Journal of Geophysical Research: Space Physics*, *120*, 7209–7227. https://doi.org/10.1002/2015JA021529

Simon, S., Saur, J., Kriegel, H., Neubauer, F., Motschmann, U., & Dougherty, M. (2011). Influence of negatively charged plume grains and hemisphere coupling currents on the structure of Enceladus' Alfvén wings: Analytical modelling of Cassini magnetometer observations. *Journal of Geophysical Research*, *116*, A04221. https://doi.org/10.1029/2010JA016338

Smith, E. J., Davis Jr., L., Jones, D. E., Coleman Jr., P. J., Colburn, D. S., Dyal, P., et al. (1974). The planetary magnetic field and magnetosphere of Jupiter: Pioneer 10. *Journal of Geophysical Research*, *79*, 3501–3513. https://doi.org/10.1029/JA079i025p03501

Sparks, W. B., Hand, K. P., McGrath, M. A., Bergeron, E., Cracraft, M., & Deustua, S. E. (2016). Probing for evidence of plumes on Europa with HST/STIS. *The Astrophysical Journal*, *829*(2), 121.

Sparks, W. B., Schmidt, B. E., McGrath, M. A., Hand, K. P., Spencer, J. R., Cracraft, M., & Deustua, S. E. (2017). Active cryovolcanism on Europa? *The Astrophysical Journal Letters*, *839*(2), L18.

Tokar, R. L., Johnson, R. E., Thomsen, M. F., Wilson, R. J., Young, D. T., Crary, F. J., et al. (2009). Cassini detection of Enceladus' cold water-group plume ionosphere. *Geophysical Research Letters*, *36*, L13203. https://doi.org/10.1029/2009GL038923

Volwerk, M., Khurana, K., & Kivelson, M. (2007). Europa's Alfven wing: Shrinkage and displacement influenced by an induced magnetic field. *Annales Geophysicae*, *25*(4), 905–914. https://doi.org/10.5194/angeo-25-905-2007

Zimmer, C., Khurana, K. K., & Kivelson, M. G. (2000). Subsurface oceans on Europa and Callisto: Constraints from Galileo magnetometer observations. *Icarus*, *147*(2), 329–347. https://doi.org/10.1006/icar.2000.6456